J. Biochem. 131, 59–69 (2002)

Effects of Hydrogen Bonds in Association with Flavin and Substrate in Flavoenzyme D-Amino Acid Oxidase. The Catalytic and Structural Roles of Gly313 and Thr317[1]

Chiaki Setoyama,[*] Yasuzo Nishina,[†] Haruhiko Tamaoki,[*] Hisashi Mizutani,[‡] Ikuko Miyahara,[‡] Ken Hirotsu,[‡] Kiyoshi Shiga,[†] and Retsu Miura[*,2]

Departments of [*]Biochemistry and [†]Physiology, Kumamoto University School of Medicine, 2-2-1 Honjo, Kumamoto 860-0811; and [‡]Department of Chemistry, Graduate School of Science, Osaka City University, Sugimoto, Sumiyoshi-ku, Osaka 558-8585

Received August 9, 2001; accepted October 24, 2001

According to the three-dimensional structure of a porcine kidney D-amino acid oxidase-substrate (D-leucine) complex model, the G313 backbone carbonyl recognizes the substrate amino group by hydrogen bonding and the side-chain hydroxyl of T317 forms a hydrogen bond with C(2)=O of the flavin moiety of FAD [Miura *et al.* (1997) *J. Biochem.* 122, 825–833]. We have designed and expressed the G313A and T317A mutants and compared their enzymatic and spectroscopic properties with those of the wild type. The G313A mutant shows decreased activities to various D-amino acids, but the pattern of substrate specificity is different from that of the wild type. The results imply that the hydrogen bond between the G313 backbone carbonyl and the substrate amino group plays important roles in substrate recognition and in defining the substrate specificity of D-amino acid oxidase. The T317A mutant shows a decreased affinity for FAD. The steady-state kinetic measurements indicate diminished activities of T317A to substrate D-amino acids. The transient kinetic parameters measured by stopped-flow spectroscopy revealed that T317 plays key roles in stabilizing the purple intermediate, a requisite intermediate in the oxidative half-reaction, and in enhancing the release of the product from the active site, thereby optimizing the overall catalytic process of D-amino acid oxidase.

Key words: D-amino acid oxidase, flavoenzyme, hydrogen bond, purple intermediate, site-specific mutation.

D-Amino acid oxidase (EC 1.4.3.3, DAO) from porcine kidney is an FAD-dependent oxidase and one of the most extensively investigated flavooxidases, and thus has been accepted as a prototype flavooxidase. The catalytic cycle of DAO consists of two half-reactions, *i.e.*, reductive and oxidative half-reactions. In the former, the substrate D-amino acid is dehydrogenated to the corresponding ketimino acid by flavin, which becomes reduced, while in the latter, reduced flavin is reoxidized by molecular oxygen for enzyme turnover. The three-dimensional structure of DAO has recently been solved by our group (*1*) and elsewhere (*2*), and we have modeled the enzyme-substrate complex by molecular mechanics simulation using the three-dimensional structure of the DAO-substrate analog complex as the starting coordinates (*3*). Furthermore, we have proposed a molecular mechanism for the reductive half-reaction on the grounds of not only the binding mode of the substrate in the active site but also the mutual positioning between the substrate D-amino acid and flavin in the DAO-substrate complex model (*3*). The molecular details of the reductive half-reaction of DAO are still a matter of controversy even after the crystal structure of DAO became available; a different mechanism from ours has been proposed on the basis of the active-site structure (*2, 4*). On the other hand, we have clarified the mode of optimization of the oxidative half-reaction by taking account of the three-dimensional structure of the purple intermediate, a requisite intermediate in the oxidative half-reaction (*5*).

Hydrogen-bonding interactions or networks thereof are widely found in biological systems. They play critical roles in static frameworks as well as in dynamic processes, including enzymatic catalyses. In flavoenzyme-catalyzed reactions, hydrogen bonds associated with flavin and with substrates are equally important both for their activation and for the mutual alignment required for catalysis. According to the DAO-substrate complex model (*3*), the substrate amino group interacts with the G313 backbone carbonyl through hydrogen-bonding (Fig. 1). We mutated the

[1]This study was supported in part by the following grants: Grants-in-Aid for Scientific Research from the Ministry of Education, Science, Sports, and Culture of Japan [No. 11133254 (Priority Areas (A)) (K.H.), No. 13125207 (Priority Areas (B)) (K.H.), No. 10146103 (Priority Areas (A)) (R.M.), No. 13125206 (Priority Areas (B)) (R.M.)], Research Grant from Japan Society for the Promotion of Science (Research for the Future) (K.H. and R.M.), Sakabe project of Tsukuba Advanced Research Alliance (K.H.).

[2]To whom correspondence should be addressed. E-mail: miura@gpo.kumamoto-u.ac.jp

Abbreviations: DAO, D-amino acid oxidase; DPC, Δ^1-pyrrolidine-2-carboxylate; HOMO, highest occupied molecular orbital; LUMO, lowest unoccupied molecular orbital; OAB, *o*-aminobenzoate.

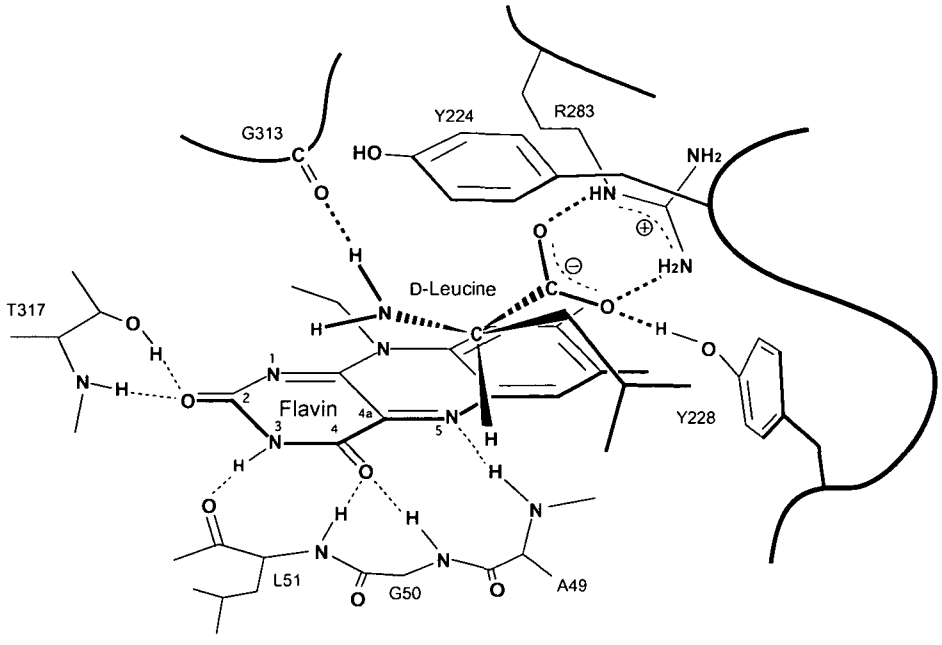

Fig. 1. **The substrate-binding mode in the DAO-D-leucine complex model (*3*) with the hydrogen-bonding network associated with flavin (*1*).**

G313 site specifically to alanine and valine to understand the effects of this hydrogen bond on the catalytic and spectroscopic properties of DAO. The three-dimensional structures of DAO (*1, 2*) revealed a unique hydrogen-bonding network between the flavin nucleus and the protein moiety (Fig. 1). Among these hydrogen bonds, the hydrogen bond between the T317 hydroxyl and the C(2)=O of flavin is removed by site-specific mutation of T317 to alanine. We report in the present study the important roles played by these hydrogen bonds or the residues responsible for these hydrogen bonds based on a comparison of the catalytic as well as static properties between the mutant and the wild-type forms of DAO.

MATERIALS AND METHODS

Wild-type DAO was obtained as previously described from *Escherichia coli* into which DAO cDNA had been incorporated by an expression vector (*6*). The concentrations of the wild-type and mutant DAOs are based on the molar absorption coefficient of 11,300 M^{-1} cm^{-1} for the 455-nm band, assuming that the molar absorption coefficient of the mutants is identical to that of the wild type. Chemicals used in this study were of the highest grade available from commercial sources and used as supplied.

The G313A and T317A mutants were constructed by a PCR method, using a system Mutan-super express km (Takara Shuzo, Kyoto). The expression plasmid pETDAO, previously described (*6*), was digested with *Xba*I and *Hin*dIII, and a 1.1-kb DNA fragment containing porcine DAO cDNA was subcloned into plasmid pKF18k (*7*) with a dual amber in the K_m gene. For the PCR reaction, oligonucleotides 5′-TGGCCATGGA***GCC***TATGGGCTCACCAT-3′ (where ***GCC*** denotes replacement of Gly313 by alanine) and 5′-CTATGGGCTC***GCC***ATCCACT-3′ (***GCC***, replacement of Thr317 by alanine) were used to obtain G313A and T317A, respectively. The mutant clones were selected by a kanamycin-resistant phenotype in MV1184 (*sup*°) cells. Taking advantage of the unique *Xba*I and *Hin*dIII restriction sites, the mutated DAO fragment was replaced into the wild-type vector. The final plasmids, pETDAO-G313A and pETDAO-T317A, were confirmed by sequencing. For the expression of these mutant enzymes, *Escherichia coli* strain BL21-(DE3) was used. Cells were grown in LB medium to an absorbance at 600 nm of 0.6. Isopropyl-1-thio-β-D-galactopyranoside was added to a final concentration of 0.01 mM, and the cells were grown for an additional 20 h before being harvested. Purification of the enzyme specimens was according to the procedures described previously (*6*).

Visible absorption spectra were obtained with a Hitachi U-3200 spectrometer thermostated at 25°C. Transient kinetic measurements were carried out with a rapid-scanning and stopped-flow spectrometer system, Otsuka Electronics RA-415S/RA-401, in 100 mM pyrophosphate buffer, pH 8.3, at 25°C. Resonance Raman spectra were measured with a JASCO NR-1800 spectrometer with a He-Ne laser as the excitation light source in 50 mM pyrophosphate buffer, pH 8.3, at room temperature (*ca.* 25°C). The wavenumber scale of the Raman spectra was calibrated with indene. Fluorescence measurement was carried out with a Hitachi F-4500 fluorescence spectrophotometer. Dissociation constants for the FAD-protein interaction in the wild-type and mutant forms of DAO were obtained by fluorometric titration; the fluorescence of the apoprotein at 330 nm with excitation at 280 nm is quenched by the addition of FAD (*8*).

^{13}C-NMR spectra were measured with a Varian UNITY Plus 500 spectrometer operating at 125.7 MHz under proton irradiation at 25°C in 50 mM pyrophosphate buffer, pH 8.3, containing 10% D_2O for field lock. The ^{13}C-chemical shift was scaled downfield in ppm from the methyl-^{13}C signal of external 3-(trimethylsilyl)propionate-d_4.

The activities of wild-type and mutant DAOs were measured by oxygen consumption with a Galvani-type oxygen electrode (Iijima Electronics) fitted in a 1.5 ml reaction vessel thermostated at 25°C. The reaction was carried out in

100 mM pyrophosphate buffer, pH 8.3, containing 20 μM FAD. The initial velocity was obtained on the basis of the oxygen concentration of 240 μM in an air-equilibrated aqueous solution at 25°C.

The transient kinetic measurement of the reaction between the purple intermediate and oxygen with D-alanine as substrate was carried out as follows. The purple intermediate was formed by reacting the enzyme (wild type, 66.7 μM, or mutant, 69.3 μM) with D-alanine (10 mM) in the presence of pyruvate (100 mM) and ammonium sulphate (100 mM) in one chamber of the stopped-flow apparatus. The purple intermediate so formed was then mixed with buffer containing different concentrations of oxygen (from 120 to 600 μM) in another chamber. The oxygen concentration was determined with the oxygen electrode. The disappearance of the purple intermediate, concomitant with the appearance of the 455 nm band of the oxidized enzyme, was followed at 560 nm by the stopped-flow spectrometer. The observed disappearance rate of the purple intermediate showed a linear dependence on oxygen concentration. The second order rate constant (k_5 in Fig. 8) was obtained from the slope of the observed rate *vs.* the oxygen concentration.

The first-order reaction rate (k_6 in Fig. 8) of the release of the product from the oxidized enzyme–ketimino acid complex was measured by stopped-flow spectroscopy. The purple intermediate was formed in one chamber following the procedure described in the previous section. The intermediate was then mixed with the buffer in the second chamber containing the buffer saturated with oxygen, *i.e.*, 1.2 mM of oxygen, and 200 mM *o*-aminobenzoate (OAB). The reaction was followed at 560 nm by the stopped-flow spectrometer. The absorbance at 560 nm decreased rapidly due to the formation of the oxidized enzyme–ketimino acid complex, and then reappeared due to the formation of the enzyme-OAB complex immediately after the release of ketimino acid from the complex. The first-order rate constant obtained from the reappearance of the 560-nm absorption represents the rate (k_6 in Fig. 8) of release of ketimino acid from the oxidized enzyme–ketimino acid complex.

The molecular mechanics simulation of the complex between *o*-aminobenzoate (OAB) and the G313A mutant was performed by the energy minimization method with XPLOR (*9*) using the atomic coordinates of the DAO-OAB complex (*3*) as the starting model.

RESULTS

Properties of the G313A Mutant; Role of the Hydrogen Bond between the G313 Backbone Carbonyl and the Substrate Amino Group—*o*-Aminobenzoate (OAB) is known to form a charge-transfer complex with flavin when it binds to the active site of DAO, the details of which were described in the crystallographic study of the DAO-OAB complex (*3*). The G313A mutant was found to bind OAB resulting in the charge-transfer complex between flavin and OAB as shown by the broad charge-transfer band in the long wavelength region beyond 500 nm (Fig. 2). The dissociation constant for the G313A-OAB complex was found to be 1.43 mM by spectroscopic titration of the charge-transfer band at 560 nm (results not shown). The dissociation constant for the wild type DAO-OAB complex was 23.3 μM, indicating that the affinity of OAB for the G313A mutant is appreciably weaker than that for the wild type. The crystal structure of the DAO-OAB complex revealed that the amino group of OAB forms a hydrogen bond with the backbone carbonyl oxygen of G313 (*3*). The binding mode of OAB in the G313A-OAB complex was modeled by the molecular mechanics simulation method with the atomic coordinates of the wild type-OAB complex as the starting structure, and the results are shown in Fig. 3 in comparison with the crystal structure of the wild type-OAB complex (*3*). Note that the loop involving A313 has moved toward the uracil edge of the flavin, probably making the hydrogen bond between the backbone carbonyl with the amino group less favorable than that in the wild type. This loop movement is apparently due to the steric effect of the methyl group of the mutated alanine. In the wild-type DAO-substrate complex model, the G313 carbonyl forms a hydrogen bond with the substrate amino group (*3*). In order to understand the catalytic effect of this hydrogen bond, we examined the enzymatic properties of the G313A mutant. Table I summarizes the steady-state kinetic constants of the mutant in comparison with those of the wild type. The mutant shows an increase in K_m and decrease in k_{cat} with all substrates examined except D-arginine, suggesting that the hydrogen bond between the substrate amino group and the backbone carbonyl of G313 is important for substrate binding as well as for positioning the substrate appropriately for the redox reaction between the flavin and the substrate.

Properties of the T317A Mutant; Role of the Hydrogen Bond between the T317 Side Chain Hydroxyl and Flavin C(2)=O—T317 participates in the hydrogen-bonding network surrounding the flavin ring at the side-chain hydroxyl and at the backbone amide group (Fig. 1). The hydrogen bond between side-chain hydroxyl and C(2)=O of flavin is

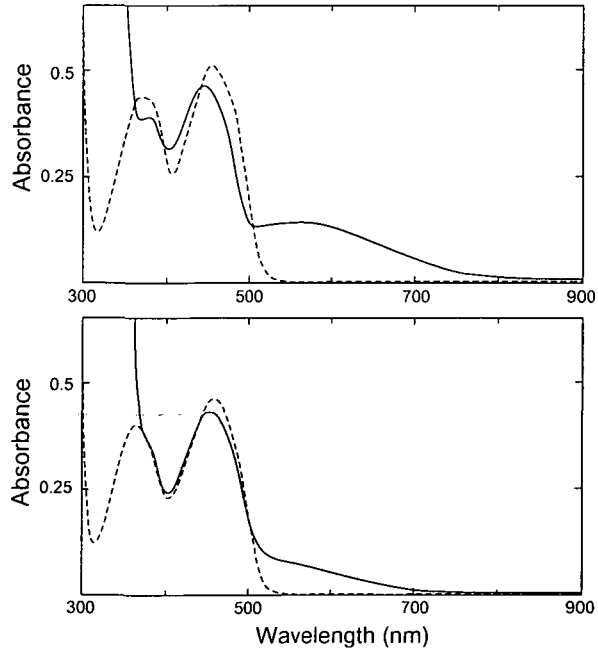

Fig. 2. **Top, absorption spectra of wild-type DAO (broken line) and its complex with OAB (solid line).** Concentrations: wild-type DAO, 45 μM; OAB, 1.7 mM. **Bottom, absorption spectra of G313A (broken line) and G313A-OAB complex (solid line).** Concentrations: G313A, 40 μM; OAB, 11 mM.

the shortest and thus the strongest among the hydrogen bonds associated with the flavin ring system (*1, 3*). In order to assess the effects of this hydrogen-bonding interaction with flavin, we removed the hydrogen bond by the site-specific mutation of T317 to alanine. The dissociation constant of FAD in the T317A mutant was found to be 8.9 μM (see "MATERIALS AND METHODS"), which is slightly larger than that in the wild type, 1.1 μM, indicating that the hydrogen bond at flavin C(2)=O with the T317 hydroxyl group contributes to the affinity of FAD for the apoprotein moiety.

It has been anticipated theoretically by molecular orbital calculations that the hydrogen-bonding network surrounding the flavin ring system alters the electronic state, and thus the catalytic properties of flavin as well (*10–12*). In order to evaluate the effect of the hydrogen bonding at flavin on the electronic state of flavin, we measured the visible absorption, resonance Raman, and ^{13}C-NMR spectra of T317A and compared them with those of the wild type, since these spectra are known to be sensitive to the electronic state of flavin.

The visible absorption spectrum of T317A differs slightly from that of the wild type; the first flavin band at 455 nm is red-shifted, while the second band around 370 nm is blue-shifted from those of the wild type (Fig. 4, top), implying the effect of the hydrogen bond at C(2)=O on the electronic state of the flavin ring. Moreover, the shoulder at about 490

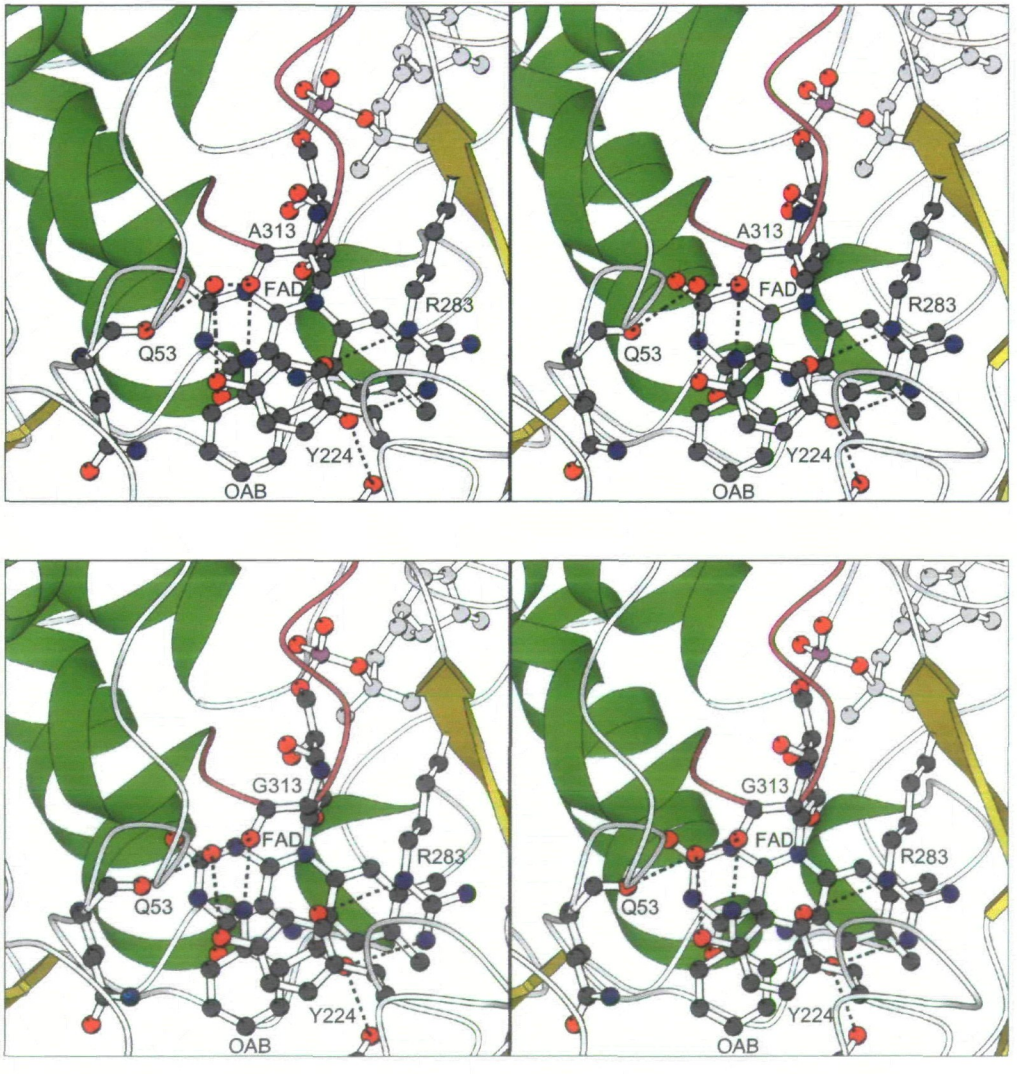

Fig. 3. **Top, stereodrawing of the OAB-binding mode in the G313A-OAB complex model obtained by molecular mechanics simulation. Bottom, stereodrawing of the OAB binding site in the crystal structure of the wild type-OAB complex (*3*).** The loop Y309–G315 including A/G313 is shown in red. Structures were constructed with the program MOLSCRIPT (*33*).

TABLE I. **Kinetic parameters of G313A in comparison with the wild type DAO.**

Substrate	K_m (mM)		k_{cat} (s^{-1})		k_{cat}/K_m (mM^{-1} s^{-1})	
	Wild type	G313A	Wild type	G313A	Wild type	G313A
D-Alanine	0.77	250	6.6	4.9	8.6	0.02
D-Proline	0.33	10.9	9.8	4.1	30	0.38
D-Arginine	11.7	14.3	3.2	3.8	0.27	0.27
D-Serine	3.6	22.7	3.1	0.75	0.86	0.003
D-Isoleucine	1.3	8.3	4.8	0.63	3.7	0.08
D-Methionine	0.14	2.0	6.5	4.35	46	2.2

nm in the mutant spectrum is slightly more prominent than that in the wild type spectrum, reflecting the more hydrophobic nature of the environment surrounding the flavin (*13*), which is consistent with the greater hydrophobicity of the side chain of the mutated alanine than that of the threonine in the wild type. Figure 4 (middle) presents the visible absorption spectrum of T317A in complex with OAB. The spectrum is characterized by the broad absorption band in the long wavelength region typical of the charge-transfer interaction with flavin, the maximum absorption being at 546 nm, which is blue-shifted from the 564 nm maximum for the wild type-OAB complex. Figure 4 (bottom) shows the purple intermediate of T317A with D-proline used as a substrate. The purple intermediate of DAO is a requisite intermediate for the oxidative half-reaction and is known to be a charge-transfer complex between anionic reduced flavin and zwitterionic ketimino acid [Δ^1-pyrrolidene-2-carboxylate (DPC) when D-proline is used as substrate] (*5, 14–17*). The charge-transfer band of the purple intermediate of T317A in the long wavelength region is as intense as that of the wild type, but the wavelength of the maximum intensity is 565 nm for T317A, which is red-shifted from the 537 nm maximum for the wild type.

The ^{13}C-NMR spectra of the T317A mutant and wild type DAO reconstituted with [2-^{13}C]FAD were measured (Fig. 5 and Table II). The chemical shift values for the mutant are all shifted to higher fields compared to those of the wild

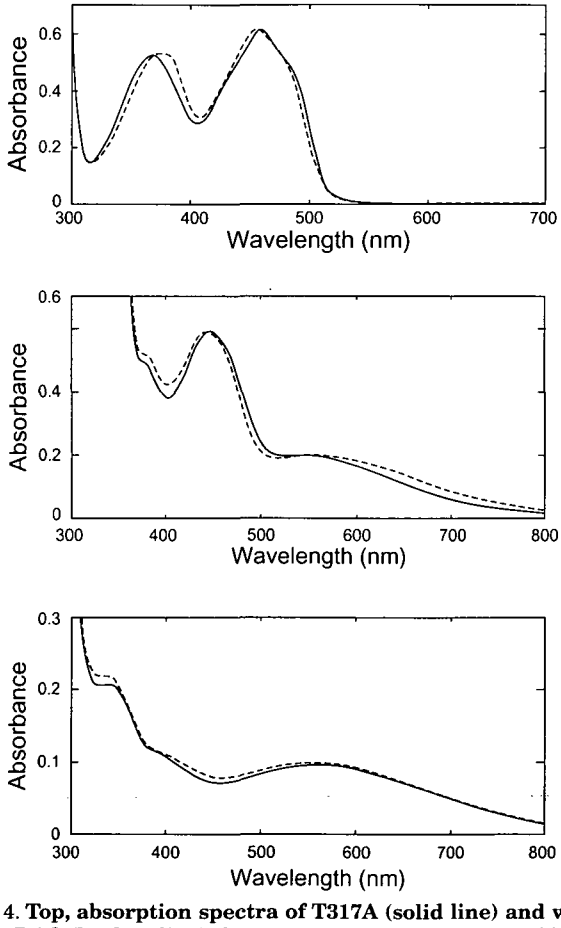

Fig. 4. **Top, absorption spectra of T317A (solid line) and wild-type DAO (broken line).** Concentrations: T317A, 54 μM; wild-type DAO, 54 μM. **Middle, absorption spectra of T317A-OAB complex (solid line) and wild type-OAB complex (broken line).** Concentrations: (solid line) G317A, 53 μM; OAB, 10 mM; (broken line) wild-type DAO, 53 μM; OAB, 10 mM. **Bottom, purple intermediate of T317A (solid line) and the wild type (broken line) with D-proline used as substrate.** The intermediate was formed by adding excess D-proline to the enzyme solution under anaerobic conditions. Concentrations: (solid line) T317A, 33 μM; D-proline, 400 mM; (broken line) wild-type DAO, 33 μM; D-proline, 400 mM.

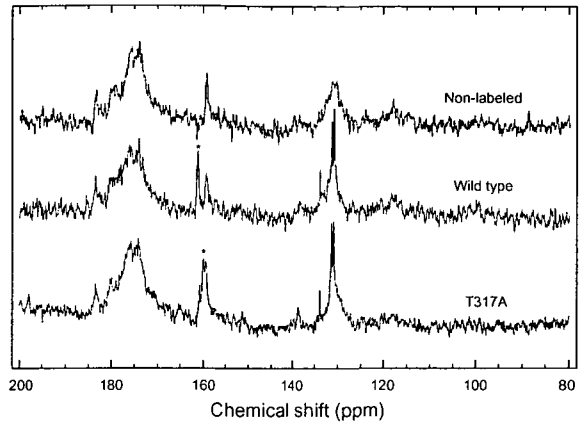

Fig. 5. **^{13}C-NMR spectra of T317A and wild-type DAO reconstituted with 2-^{13}C-labeled FAD.** Concentrations: T317A, 0.8 mM; wild-type DAO, 0.6 mM. The ^{13}C(2) signals are designated by asterisks.

TABLE II. **^{13}C(2)-chemical shift values of T317A and wild type DAO reconstituted with 2-^{13}C-labeled FAD.**

	Wid type	T317A[a]
Oxidized form (free)	160.5	159.4 (−1.1)
Oxidized form (benzoate bound)	161.3	160.1 (−1.2)
Reduced form (free)	159.8	159.3 (−0.5)

[a]Values in parentheses are differences from the wild type.

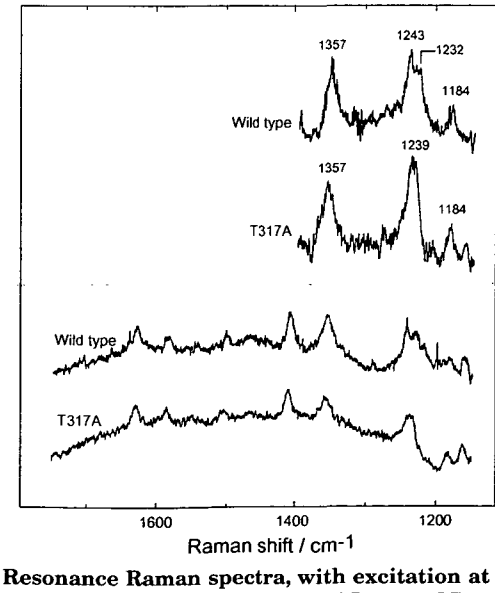

Fig. 6. **Resonance Raman spectra, with excitation at 488 nm, of T317A-OAB (T317A, *ca.* 0.6 mM; OAB, 3.3 mM) and wild-type DAO-OAB (wild-type DAO, *ca.* 0.6 mM; OAB, 2.5 mM) complexes.**

type, indicating that the chemical shift of C(2) of the flavin is sensitive to the hydrogen bond at C(2)=O and that the hydrogen bond shifts the C(2) chemical shift downfield probably by lowering the electron density at C(2).

Resonance Raman spectra of the T317A-OAB and the wild-type DAO-OAB complexes with excitation at 488 nm are presented in Fig. 6. It has been demonstrated experimentally that the band appearing in the region 1,240–1,265 cm^{-1} is sensitive to hydrogen-bonding in the uracil moiety of flavin (*18*). This band, which is designated band X according to the mode numbering by Bowman and Spiro (*19*), involves stretching modes of the C(4)-N(3) and C(2)-N(3) bonds coupled with a bending mode of the N(3)-H group (*20–22*) and increases in band frequency as the number of hydrogen bonds at the uracil moiety increases (*18, 22*). In line with this notion, the band X for the T317A mutant lacking a hydrogen bond at C(2)=O was observed at 1,239 cm^{-1}, which is low-frequency shifted from 1,243 cm^{-1} for the wild type. Figure 7 depicts the dependence of the band X frequency on the number of hydrogen bonds associated with the uracil ring portion of flavin.

In order to assess the effect of the hydrogen bond between C(2)=O and the hydroxyl group of T317 on the catalytic competence of DAO, we compared the steady-state as well as transient kinetic properties of the T317A mutant with those of the wild type. The steady state kinetic parameters obtained are summarized in Table III. We measured these kinetic parameters for the wild type and the mutant using D-alanine and D-valine as substrates at different oxygen concentrations (from 170 to 720 μM) (results not shown). But they showed no dependence on the oxygen concentration, implying that oxygen at these concentrations is kinetically saturated or reoxidation of the reduced enzyme by oxygen is not rate-limiting under the conditions employed. The catalytic efficiency as expressed by k_{cat}/K_m is smaller for the T317A mutant than that for the wild type with all substrates examined, indicating that the hydrogen bond between the T317 hydroxyl and flavin C(2)=O does indeed play a favorable role in catalysis. In order to understand to which elementary process the hydrogen bond in question contributes, we carried out a transient kinetic study by stopped-flow spectroscopic measurements. Figure 8 depicts the catalytic cycle of DAO and the rate constant for each elementary process (*23, 24*). At the end of the reductive half-reaction, the purple intermediate is formed; the process up to the formation of the purple intermediate is the reductive half-reaction. Thus, the rate of formation of the purple intermediate is taken as the apparent rate, k^r_{obs}, for the reductive half-reaction (*23, 24*) and k^r_{obs} can be measured by following the charge-transfer band in the long wavelength region. As described above, the purple intermediate is characterized by a broad charge-transfer band extending beyond 700 nm (Fig. 4, bottom). Figure 9 (top) shows the stopped-flow traces of the purple-intermediate formation as measured by the increase in the charge-transfer band at 560 nm for the wild-type and T317A mutant DAO with 5 mM D-alanine. These traces are expressed by similar first-order rate constants, k^r_{obs}, of 62 and 55 s^{-1} for the wild type and mutant, respectively. The formation of the purple intermediate was also followed with 2.5 and 0.5 mM D-alanine. The k^r_{obs} values of the wild type with 2.5 and 0.5 mM D-alanine were 35 and 7.7 s^{-1}, respectively, and the corresponding k^r_{obs} values of the mutant were 27 and 7.7 s^{-1}, respectively. These observations indicate that k^r_{obs} of the mutant is practically the same as that of the wild type regardless of the concentration of the substrate D-alanine.

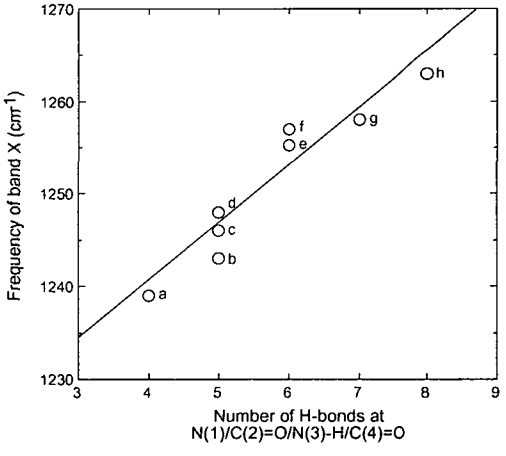

Fig. 7. **Plot of the band X frequency against the number of hydrogen bonds at the uracil moiety of the flavin ring.** Data for wild-type DAO (b) and the T317A mutant (a) were added to the plot adopted from Tegoni *et al.* (*18*). Data points are: c, glutathione reductase; d, glucose oxidase; e, short-chain acyl-CoA dehydrogenase; f, *Desulfovibrio vulgaris* falvodoxin, flavocytochrome b_2, medium-chain acyl-CoA dehydrogenase (*34*); g, *p*-hydroxybenzoate hydroxylase; h, old yellow enzyme.

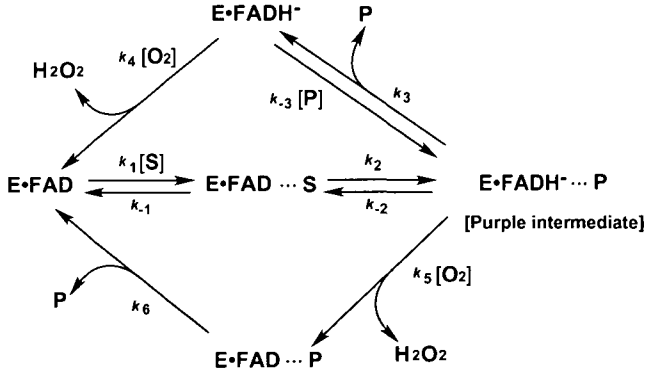

Fig. 8. **Catalytic cycle of DAO.** S and P represent substrate D-amino acid and product ketimino acid, respectively.

TABLE III. **Steady-state kinetic parameters of wild-type DAO and the T317A mutant.**

Substrate	K_m (mM)		k_{cat} (s^{-1})		k_{cat}/K_m (mM^{-1} s^{-1})	
	Wild type	T317	Wild type	T317	Wild type	T317
D-Alanine	1.1	1.0	8.5	0.92	7.7	0.92
D-Proline	1.1	1.2	21	9.7	19	8.1
D-Serine	4.8	20.8	2.7	1.8	0.56	0.09
D-Valine	0.67	4.3	2.5	0.90	3.7	0.21
D-Phenylalanine	1.4	9.1	17	2.4	12	0.26

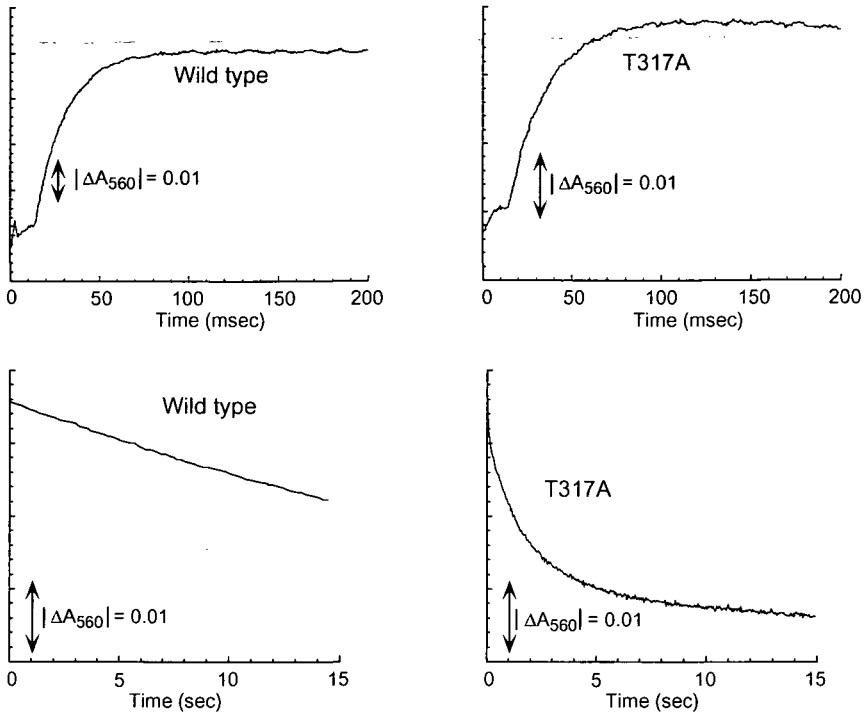

Fig. 9. **Top, stopped-flow measurement of formation of the purple intermediate as monitored by the absorbance increase at 560 nm in the anaerobic reaction of D-alanine with wild-type DAO (left) or T317 mutant (right).** The reaction was initiated by adding of 5 mM (final concentration) D-alanine to T317A (30 μM, final concentration) or wild-type DAO (30 μM, final concentration). **Bottom, stopped-flow measurement of the decay of the purple intermediate as monitored by the absorbance decrease at 560 nm in the anaerobic reaction of D-alanine with wild-type DAO (left) or T3177A mutant (right).** Reaction conditions were the same as above. Note that the time scale is large to monitor the decay of the purple intermediate by the decrease of the charge-transfer band at 560 nm.

TABLE IV. **The reaction rate constants obtained by transient kinetic measurement with D-alanine used as substrate.**

Rate constants[a]	Wild type	T317A
k^r_{obs}/s^{-1}	62	55
k_3/s^{-1}	0.036	0.40
$k_4/M^{-1}\ s^{-1}$	1.6×10^4	1.1×10^4
$k_5/M^{-1}\ s^{-1}$	1.3×10^5	1.9×10^5
k_6/s^{-1}	8.6	1.9

[a]The rate constant k^r_{obs} is described in the text; other rate constants are defined in the legend to Fig. 8.

These results are contrary to the expectation that the hydrogen bond at C(2)=O increases the electron acceptability as predicted by molecular orbital calculations (*12*), and that the mutant would show smaller k^r_{obs}. We then studied the stability of the purple intermediate by following the release of the product, ketimino acid. The results are shown in Fig. 9 (bottom) and the two traces are described by the first-order rate constants, k_3, of 0.036 and 0.40 s^{-1} for the wild type and the mutant, respectively. The k_3 values of the wild type with 2.5 and 0.5 mM D-alanine were 0.036 and 0.035 s^{-1}, respectively, and the corresponding values for the mutant were 0.41 and 0.37 s^{-1}, respectively. These results indicate that the purple intermediate of the mutant is less stable than that of the wild type and that T317 contributes to the stabilization of the purple intermediate. We also measured the second-order rate constants, k_4 and k_5, for the reaction of the free reduced enzyme and the purple intermediate, respectively, toward molecular oxygen (results not shown). The method of k_5 measurement is described in "MATERIALS AND METHODS." Finally, we measured the remaining rate constant, k_6 in Fig. 8 (results not shown); the method of measurement is essentially according to Porter *et al.* (*24*) and is described in "MATERIALS AND METHODS." The rate constants obtained by the stopped-flow measurements are summarized in Table IV. Each of the second-order rate constants, k_4 and k_5, of the wild type and the mutant are identical to each other within experimental error. Among the rate constants examined, k_3 and k_6 are the only ones that differ between the wild type and the T317A mutant.

DISCUSSION

The enthalpy of hydrogen-bond cleavage is within the range that can be obtained under physiological conditions. Thus the formation and modulation of hydrogen-bonding networks in the frameworks of biological systems take place statically, dynamically or transiently, and often play critical roles in these systems. In the present report we studied the effect of the hydrogen bonds associated with the substrate amino group and with the C(2)=O of the flavin ring system on the catalysis of DAO.

The hydrogen bond between the substrate amino group and the backbone carbonyl of G313 was modified by site-specific mutation of G313 to alanine. When compared with the wild type, G313A exhibits decreased catalytic efficiency, expressed as k_{cat}/K_m, toward all the substrates examined (Table I) except D-arginine for which G313A has comparable catalytic efficiency. Moreover, the mutant exhibits different substrate specificity from that of the wild type. D-Arginine shows very poor affinity for wild-type DAO and thus a high K_m value for the wild type as supported by the hydrophobic environment, surrounding the substrate side chain, which cannot well accommodate the ionic side chain of D-arginine (*3*). The comparable catalytic efficiency of G313A toward D-arginine can therefore be explained by the poor affinity of the wild type toward D-arginine; the catalytic efficiency of the wild type toward D-arginine does not seem to depend so much on the alignment of the substrate in the active site. The results of the molecular mechanics simulation of the G313A-OAB complex (Fig. 4) disclose the

movement of the loop Y309-G315, which involves A313, in the direction of the uracil moiety of flavin. This movement then distorts the carbonyl group away from the favorable position for hydrogen bonding with the amino group of OAB and therefore the substrate amino group. This deviation can explain the poor catalytic efficiency as well as the alteration in the substrate specificity of the mutant from that of the wild type (Table I). The decreased catalytic efficiency and the different substrate specificity of the mutant suggest that G313, and thus the hydrogen bond between the substrate amino group and the backbone carbonyl of G313, play important roles not only in catalytic efficiency by positioning the substrate for favorable orientation for catalysis, but also for substrate specificity. The blue shift and the decrease in the charge-transfer band of G313A-OAB as compared with those of the wild type (Fig. 2) cannot be interpreted unequivocally on a theoretical ground at present. The somewhat more hydrophobic environment of the active site of the mutant due to the additional methyl group in G313A may have some effect. Answering these unanswered questions may be helped by the detailed three-dimensional structure of the mutant. However, the inability of the mutant to form good quality crystals has hampered the crystallographic study of the mutant. We have also mutated G313 to valine (results not shown). The G313V mutant shows very poor affinity for FAD as well as very poor activity toward various substrate D-amino acids. In view of the profound influence of the G313A mutation on the catalytic efficiency as well as on the active-site structure (Fig. 3), the bulky side chain of valine should result in severe damage to the active site, and hence to the enzymatic activity.

The effects of the hydrogen bond at C(2)=O of the flavin with the side chain hydroxyl of T317 on various spectroscopic properties agree with the molecular orbital calculations (*10–12*) as well as chemical intuition or empirical rules. The dissociation constant of T317A-FAD is greater than that of the wild type-FAD, indicating that this hydrogen bond contributes to the affinity of FAD for the apoprotein moiety. The blue shift of the charge-transfer band of the T317A-OAB complex from that of the wild type-OAB complex (Fig. 4, middle) is reasonable in view of the prediction by molecular orbital calculations that the hydrogen bonding at C(2)=O of flavin lowers the energy level of the LUMO of oxidized flavin (*10, 12*). The transition energy for charge-transfer is correlated with the ionization potential of an electron donor, I_D, and the electron affinity of an electron acceptor, E_A, according to Eq. 1 (*25, 26*),

$$h\,\nu_{CT} = I_D - E_A - W \quad (1)$$

where h and ν_{CT} are the Planck constant and the frequency of the charge-transfer band, respectively, and W is basically the difference in the electrostatic interaction between the donor and acceptor in the ground and excited states. In the charge-transfer interaction of the DAO-OAB complex, OAB acts as the donor and oxidized flavin as the acceptor (*3, 27*). The hydrogen bond between the T317 hydroxyl and the C(2)=O of flavin is expected to lower the LUMO of oxidized flavin and thus to increase the electron affinity, E_A, of oxidized flavin. This should result in a decrease in the transition energy and shift the charge-transfer band to a lower frequency or a longer wavelength. Elimination of this hydrogen bond in the T317A mutant should, therefore, shift the charge-transfer band to a shorter wavelength in agreement with the experimental results that the charge-transfer band of the wild type-OAB was found at 564 nm while that of T317A-OAB was found at 546 nm (Fig. 4, middle). The purple intermediate of DAO has been demonstrated as the charge-transfer complex between the zwitterionic ketimino acid, DPC, when D-proline is used as substrate, as acceptor and anionic reduced flavin as donor (*5, 14–17*). That the charge-transfer band at 537 nm for the purple intermediate of the wild type is found at a shorter wavelength than the 565 nm for T317A (Fig. 4, bottom) can be regarded in the context of the theoretical prediction from molecular orbital calculations (*11*), according to which the hydrogen bond at C(2)=O of flavin reduces the energy level of the highest occupied molecular orbital (HOMO) of reduced flavin (*11*) and thus increases the ionic potential I_D of reduced flavin thereby shifting the charge-transfer band to a higher frequency or to a shorter wavelength (Eq. 1). The removal of the hydrogen bond at C(2)=O in T317A should accordingly shift the charge-transfer band to a longer wavelength, which agrees with the experimental results. These results prove experimentally the theoretical prediction that the hydrogen bond at C(2)=O does lower the energy levels of the LUMO and HOMO of the oxidized flavin and the reduced flavin, respectively (*11*). The ^{13}C-NMR study of the wild type and T317A mutant show that the ^{13}C-chemical shift of flavin C(2) is sensitive to the hydrogen bond at C(2)=O with the T317 hydroxyl and undergoes low-field shift from that without hydrogen-bond (Table II). This agrees with the chemical intuition that a hydrogen bond at a carbonyl oxygen reduces the electron density at the carbon, thereby shifting the chemical shift to a lower field. Modulation of a hydrogen bond at flavin C(2)=O during flavoenzyme catalysis or in flavoenzyme complexed with an effector can thus be probed by the ^{13}C-chemical shift of the carbonyl carbon. The resonance Raman spectra of the wild type-OAB and the T317A-OAB complexes with excitation within the charge-transfer band gave results in support of the empirical correlation (*18*) between band X (*19*) of flavin and the number of hydrogen bonds at the uracil portion of the flavin (Fig. 7). Because band X derives from a mixture of a few vibrational modes (see "RESULTS"), the dependence of band X on the number of hydrogen bonds at the uracil ring moiety cannot be explained purely on theoretical grounds. However, the dependence shown in Fig. 7 implies that band X can serve as a reporter for the modulation of the hydrogen-bonding network at the flavin ring, which is regarded as one of the most important factors controlling the catalytic events of flavoenzymes.

Since a hydrogen bond at C(2)=O of oxidized flavin is predicted to increase the electron acceptability by lowering the energy level of the LUMO, the steady-state kinetic properties of the T317A mutant in comparison with those of the wild type were thought to derive from a higher reaction rate, k^r_{obs}, for the reductive half-reaction of the wild type. However, the transient kinetic experiments gave unexpected results. The value of k^r_{obs}, the rate constant for the formation of the purple intermediate or the apparent rate constant for the reductive half-reaction, of T317A is practically identical to that of the wild type (Fig. 9, top, and Table IV). These results indicate that lowering the energy level of the LUMO of oxidized flavin by the hydrogen bond at C(2)=O with the T317 hydroxyl group is not strong enough

to influence the reaction rate of the reductive half-reaction. Further transient kinetic analysis indicated that the favorable steady state property of the wild type over the mutant is achieved by the greater stability of the purple intermediate and faster release of the product in the wild type than in the mutant, as demonstrated by the smaller decay constant, k_3, of the purple intermediate and greater k_6 value of the wild type than those of the mutant (Fig. 9, bottom, and Table IV). The reactivities of the free reduced form and the purple intermediate of the wild type toward oxygen are essentially the same as the corresponding rates of the mutant, respectively (Table IV). But the reactivity of the purple intermediate toward oxygen (k_5) is greater than that of the free reduced form (k_4) in both the wild type and mutant enzymes. The slower steady state reaction of the mutant can now be qualitatively interpreted by a combination of the greater value of k_3 and the smaller value of k_6 of the mutant than the wild type. During the steady state catalysis of the mutant, the fraction of the free reduced form, with poor reactivity with oxygen, may not be negligible due to the faster decay of the purple intermediate. Furthermore, the steady state reaction of the mutant is retarded by the slower release of the product, ketimino acid, from the oxidized enzyme-product complex during the final stage of the oxidative half-reaction. It is, therefore, concluded that T317 plays a unique dual role in stabilizing the purple intermediate, a requisite intermediate in the oxidative half-reaction, on the one hand, and destabilizing the oxidized enzyme-product complex on the other. The interpretation of the steady-state kinetics in terms of the microscopic rate constants obtained by transient kinetics remains qualitative in this report, the main reason being that DAO exists in a concentration-dependent self-associating equilibrium among monomer, dimer, tetramer, hexamer, octamer, ... (*28, 29*), and that the enzymatic properties differ appreciably between the monomer and oligomers/polymers (*30*). The purely quantitative description of the steady-state kinetics in terms of the microscopic constants should incorporate the self-associating equilibrium with different steady-state as well as transient kinetic constants for monomer and oligomers/polymers of the wild type and mutant. However, a semi-quantitative description of the steady state k_{cat} in terms of the transient kinetic constants can be attempted based on the assumption that the kinetic constants, be they steady-state or transient, are not dependent on the self-associating equilibrium. The steady-state rate constant, k_{cat}, can then be expressed as in Eq. 1

$$k_{cat} = (k_3 + k_5[O_2])/(1 + k_3/k_4[O_2] + k_5[O_2]/k_6) \quad (2)$$

where $[O_2]$ is 240 μM. The values of k_{cat} calculated for the wild type and mutant are 6.7 and 1.8 s^{-1}, respectively, which agree well with the observed values, 8.5 and 0.92 s^{-1}, respectively (Table III). In these calculations, the contributions of k_3 in the numerator and $k_3/k_4[O_2]$ in the denominator in Eq. 2 are negligible, so that k_{cat} can be approximated as

$$k_{cat} = (k_5[O_2])/(1 + k_5[O_2]/k_6)$$

This implies that the inefficient steady state rate of the mutant is semi-quantitatively explained mainly by the retarded release of the product from the oxidized enzyme-product complex.

The three-dimensional structure of the purple intermediate has recently been solved by us and the mode of the charge-transfer interaction as well as the optimization mechanism of the oxidative half-reaction were clarified (*5*). To understand the unique role played by T317 in stabilizing the purple intermediate, we looked more carefully into the structural features surrounding T317 of the purple intermediate. In addition to the hydrogen bond to flavin C(2)=O, the hydroxyl group of T317 is also hydrogen-bonded to the backbone amide of Q53, which is in the loop forming hydrogen-bonding network with the flavin ring (Fig. 10). Moreover, T317 is located toward the N-terminal

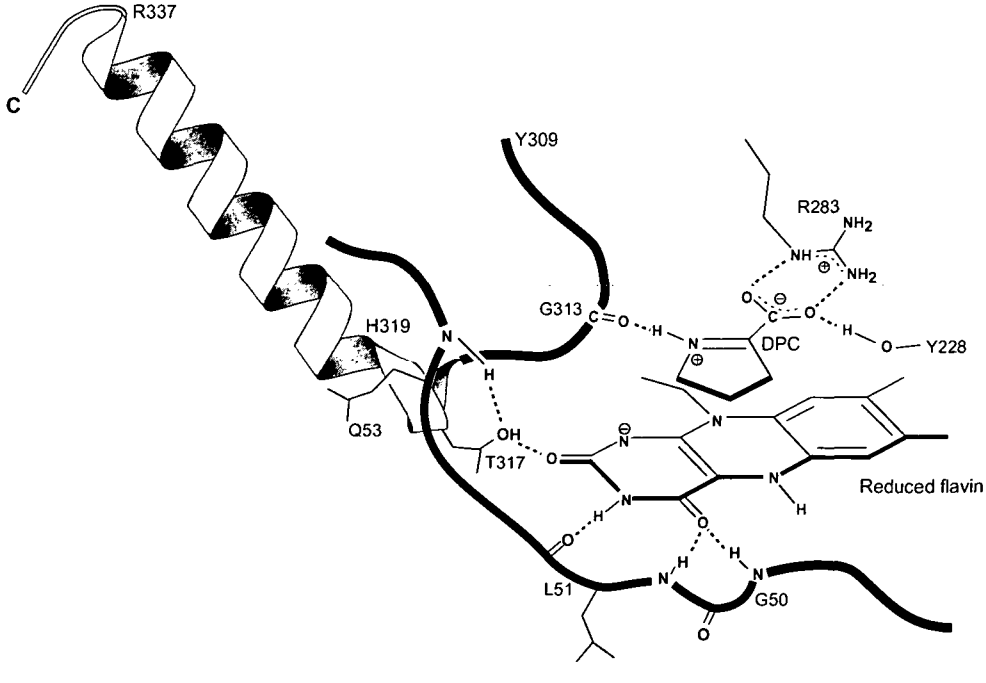

Fig. 10. **Illustration of the active site of the purple intermediate (*5*) featuring the connecting role of T317 between loops and a helix.** The structure of the helix was constructed with the program MOLSCRIPT (*33*).

end of the C-terminal helix (G315–R337), which has a characteristic kink at H319. Through the hydrogen-bonding network, T317 therefore connects the flavin ring, the α-helix G315–R337, and the loop responsible for the hydrogen-bonding network with the uracil portion of flavin. The connecting region between the loop Y309–G315 and helix G315–R337 is rich in glycine residues (G312-G313-Y314-G315). This glycine-rich region and the kink in the helix at H319 imply a constrained structure around these regions. T317 is located at the center of the constrained structure and seems to play a major role in the strain. Mutation of T317 to alanine disrupts the hydrogen-bonding network connecting the helix and the two loops and may release the strain to straighten the kink at H319 in the helix. This would then result in movement of the loop containing G313, and thus in unfavorable hydrogen bonding between the protonated ketimino nitrogen and the backbone carbonyl of G313 in the purple intermediate (*5*) to bring instability to the purple intermediate. Molecular mechanics simulation of T317A to prove this notion probably would not give reliable results, since the large perturbation produced by the mutation is considered to be beyond the limits allowed for simulation. It should be emphasized that T317 is conserved in pig, human, mouse, rabbit, and rat DAOs, all the mammalian DAOs whose primary structures are known (*31, 32*). In fact, both the stretches Y309–A323, which includes the loop involving G313 and the part of the helix containing the kink, and D46-S57, which includes Q53 and the backbone hydrogen-bonded to flavin, are conserved in all mammalian DAOs, suggesting the importance of the network shown in Fig. 10 in catalysis and/or maintenance of the active-site structure.

Another unique role played by T317 is destabilizing the oxidized enzyme-product complex and thus enhancing the product release in the final stage of the oxidative half-reaction. The secondary structural effect due to the release of the strain shown in Fig. 10 in the active site of the mutant may result in more favorable complex formation of ketimino acid with the oxidized form of the mutant than with that of the wild type. Unfortunately, we do not have a firm theoretical basis for explaining this role, mainly due to the lack of structural information about the oxidized enzyme-ketimino acid complex. When the oxidized form of DAO is saturated with the product, ketimino acid, the ketimino acid bound to the active site gradually turns to enamino acid (*34*). Crystallographic analysis of the oxidized enzyme-ketimino acid is, therefore, probably impossible. However, clues to the precise role of the network shown in Fig. 10 may be found by crystallographic analysis of the mutant, an issue for future study.

REFERENCES

1. Mizutani, H., Miyahara, I., Hirotsu, K., Nishina, Y., Shiga, K., Setoyama, C., and Miura, R. (1996) Three-dimensional structure of porcine kidney D-amino acid oxidase at 3.0 Å resolution. *J. Biochem.* **120**, 14–17
2. Mattevi, A., Vanoni, M.A., Todone, F., Rizzi, M., Teplyakov, A., Coda, A., Bolognesi, M., and Curti, B. (1996) Crystal structure of D-amino acid oxidase: A case of active site mirror-image convergent evolution with flavocytochrome b_2. *Proc. Natl. Acad. Sci. USA* **93**, 7496–7501
3. Miura, R., Setoyama, C., Nishina, Y., Shiga, K., Mizutani, H., Miyahara, I., and Hirotsu, K. (1997) Structural and mechanistic studies on D-amino acid oxidase·substrate complex: Implications of the crystal structure of enzyme·substrate analog complex. *J. Biochem.* **122**, 825–833
4. Mattevi, A., Vanoni, M.A., and Curti, B. (1997) Structure of D-amino acid oxidase: new insight from an old enzyme. *Curr. Opin. Struct. Biol.* **7**, 804–810
5. Mizutani, H., Miyahara, I., Hirotsu, K., Nishina, Y., Shiga, K., Setoyama, C., and Miura, R. (2000) Three dimensional structure of the purple intermediate of porcine kidney D-amino acid oxidase. Optimization of the oxidative half-reaction through alignment of the product with reduced flavin. *J. Biochem.* **128**. 73–81
6. Setoyama, C., Miura, R., Nishina, Y., Shiga, K., Mizutani, H., Miyahara, I., and Hirotsu, K. (1996) Crystallization of expressed porcine kidney D-amino acid oxidase and preliminary X-ray crystallographic characterization. *J. Biochem.* **119**, 1114–1117
7. Hashimoto-Gotoh, H., Mizuno, T., Ogasahara, Y., and Nakagawa, M. (1995) An oligodeoxyribonucleotide-directed dual amber method for site-directed mutagenesis. *Gene* **152**, 271–275
8. Tu, S.-C., Edelstein, S.J., and McCormick, D.B. (1973) A modified purification method and properties of pure porcine kidney D-amino acid oxidase. *Arch. Biochem. Biophys.* **159**, 889–896
9. Brünger, A.T., Kuriyan, J., and Karplus, M. (1987) Crystallographic *R* factor refinement by molecular dynamics. *Science* **235**, 458–460
10. Nishimoto, K., Watanabe, Y., and Yagi, K. (1978) Hydrogen bonding of flavoprotein. I. Effect of hydrogen bonding on electronic spectra of flavoprotein. *Biochim. Biphys. Acta* **526**, 34–41
11. Nishimoto, K., Kai, E., and Yagi, K. (1984) Hydrogen bonding of flavoprotein. II. Effect of hydrogen bonding at hetero atoms of reduced flavin on its reactivity. *Biochim. Biophys. Acta* **802**, 321–325
12. Nishimoto, K., Fukunaga, H., and Yagi, K. (1986) Studies in a model system on the effect of hydrogen bonding at hetero atoms of oxidized flavin on its electron acceptability. *J. Biochem.* **100**, 1647–1653
13. Müller, F. (1991) Free flavins: syntheses, chemical and physical properties in *Chemistry and Biochemistry of Flavoenzymes* (Müller, F., ed.) Vol. I, pp. 1–71, CRC Press, Boca Raton, Ann Arbor, Boston
14. Nishina, Y., Shiga, K., Watari, H., Miura, R., Miyake, Y., Tojo, H., and Yamano, T. (1982) Resonance Raman study on the purple intermediates of the flavoenzyme D-amino acid oxidase. *Biochem. Biophys. Res. Commun.* **106**, 818–822
15. Nishina, Y., Shiga, K., Miura, R., Tojo, H., Ohta, M., Miyake, Y., Yamano, T., and Watari, H. (1983) On the structures of flavoprotein D-amino acid oxidase purple intermediates. A resonance Raman study. *J. Biochem.* **94**, 1979–1990
16. Miura, R., Nishina, Y., Ohta, M., Tojo, H., Shiga, K., Watari, H., Yamano, T., and Miyake, Y. (1983) Resonance Raman study on the flavin in the purple intermediates of D-amino acid oxidase. *Biochem. Biophys. Res. Commun.* **111**, 588–594
17. Miura, R. and Miyake, Y. (1987) ^{13}C-NMR studies on the reaction intermediates of porcine kidney D-amino acid oxidase reconstituted with ^{13}C-enriched flavin adenine dinucleotide. *J. Biochem.* **102**, 1345–1354
18. Tegoni, M., Gervais, M., and Desbois, A. (1997) Resonance Raman study on the oxidized and anionic semiquinone forms of flavocytochrome b_2 and L-lactate monooxygenase. Influence of the structure and environment of the isoalloxazine ring on the flavin function. *Biochemistry* **36**, 8932–8946
19. Bowman, W.D. and Spiro, T.G. (1981) Normal mode analysis of lumiflavin and interpretation of resonance Raman spectra of flavoproteins. *Biochemistry* **20**, 3313–3318
20. Nishina, Y., Kitagawa, T., Shiga, K., Horiike, K., Matsumura, Y., Watari, H., and Yamano, T. (1978) Resonance Raman spectra of riboflavin and its derivatives in the bound state with egg riboflavin binding proteins. *J. Biochem.* **84**, 925–932
21. Abe, M. and Kyogoku, Y. (1987) Vibrational analysis of flavin derivatives: normal coordinate treatment of lumiflavin. *Spectrochim. Acta* **43A**, 1027–1037
22. Lively, C.R. and McFarland, J.T. (1990) Assignment and the

effect of hydrogen bonding on the vibrational normal modes of flavins and flavoproteins. *J. Phys. Chem.* **94**, 3980–3994
23. Bright, H.J. and Porter, D.J.T. (1975) Flavoprotein oxidases in *The Enzymes* (Boyer, P.D., ed.) Vol. 12, pp. 421–505, Academic Press, New York, San Francisco, London
24. Porter, D.J.T., Voet, J.G., and Bright, H.J. (1977) Mechanistic features of the D-amino acid oxidase reaction studied by double stopped flow spectrophotometry. *J. Biol. Chem.* **252**, 4464–4473
25. Mulliken, R.S. (1952) Molecular compounds and their spectra. III. The interactions of electron donors and acceptors. *J. Phys. Chem.* **56**, 801–822
26. Mulliken, R.S. and Person, W.S. (1969) *Molecular Complexes*, Wiley-Interscience, New York, London, Sydney, Toronto
27. Nishina, Y., Sato, K., Miura, R., and Shiga, K. (1995) Structure of charge-transfer complexes of flavoenzyme D-amino acid oxidase: A study by resonance Raman spectroscopy and extended Hückel molecular orbital method. *J. Biochem.* **118**, 614–620
28. Tojo, H., Horiike, K., Shiga, K., Nishina, Y., Watri, H., and Yamano, T. (1985) Self-association mode of a flavoenzyme D-amino acid oxidase from hog kidney. I. Analysis of apparent weight-average molecular weight data for the apoenzyme in terms of models. *J. Biol. Chem.* **260**, 12607–12614
29. Tojo, H., Horiike, K., Shiga, K., Nishina, Y., Watri, H., and Yamano, T. (1985) Self-association mode of a flavoenzyme D-amino acid oxidase from hog kidney. II. Stoichiometry of holoenzyme association and energetics of subunit association. *J. Biol. Chem.* **260**, 12615–12621
30. Shiga, K. and Shiga, T. (1972) The kinetic features of monomers and dimers in high- and low-temperature conformational states of D-amino acid oxidase. *Biochim. Biophys. Acta* **263**, 294–303
31. Miyake, Y., Fukui, K., Momoi, K., Watanabe, F., Tada, M., Miyano, M., and Takahashi, S. (1991) Molecular biochemical studies on structure-function relationship of D-amino acid oxidase in *Flavins and Flavoproteins 1990* (Curti, B., Ronchi, S., and Zanetti, G., eds.) pp. 135–142, Walter de Gruyter, Berlin, New York
32. Konno, R. (1998) Rat D-amino-acid oxidase cDNA: rat D-amino-acid oxidase as an intermediate form between mouse and other mammalian D-amino-acid oxidases. *Biochim. Biophys. Acta* **1395**, 165–170
33. Kraulis, P.J. (1991) MOLSCRIPT: A program to produce both detailed and schematic plots of protein structures. *J. Appl. Crystallogr.* **24**, 946–950
34. Hazekawa, I., Nishina, Y., Sato, K., Shichiri, M., and Shiga, K. (1995) Substrate activating mechanism of short-chain acyl-CoA, medium-chain acyl-CoA, long-chain acyl-CoA, and isovaleryl-CoA dehydrogenase. *J. Biochem.* **118**, 900–910